LARGE-EDDY SIMULATIONS OF THE BAROCLINIC MIXED LAYER

ZBIGNIEW SORBJAN*
Department of Physics, Marquette University, Milwaukee, WI 53201, U.S.A.

(Received in final form 11 August 2003)

Abstract. The effects of baroclinicity, imposed on the dry mixed layer by the presence of large-scale, horizontal temperature gradients, have been investigated based on a large-eddy simulation model. The purpose of this investigation is to examine simultaneous impacts of thermal stratification and shear in the atmospheric boundary layer. For this purpose, five cases are considered – one barotropic, and four baroclinic. Based on the performed simulations, a new parametrization of the interfacial layer is proposed. The parameterization employs new interfacial scaling, which is valid at the top of the mixed layer. In terms of new scales, dimensionless moments characterizing turbulence at the top of the shearless mixed layer are universal constants. In the sheared case, dimensionless statistics of turbulence are shown to be functions of the interfacial Richardson number.

Keywords: Atmospheric mixed layer, Baroclinicity, Convection, Entrainment, Large-eddy simulations, Shear.

1. Introduction

The present understanding of the atmospheric boundary layer (ABL) has been largely achieved as a result of large-eddy simulations (LES). The technique was introduced in the 1970s by Deardorff (1970, 1972, 1973a, b, 1974a, b). Most LES have focused on the convective mixed layer, driven by both surface heating and wind shear (Schemm and Lipps, 1976; Moeng, 1984; Nieuwstadt and Brost, 1986; Schmidt and Schumann, 1989; Mason, 1989; Moeng and Sullivan, 1994). The LES technique was also employed to simulate the stably stratified flows in the ABL (Mason and Derbyshire, 1990; Andren, 1995; Kosovic and Curry, 1999; Cedeval and Street, 1999; Saiki et al., 1999). Other LES simulations considered the impacts of stratocumuli and cumuli clouds (Deardorff, 1976; Sommeria, 1976; Moeng, 1986; Cuijpers and Duynkerke, 1993; Brown, 1999; Chlond and Wolkau, 2000; Stevens et al., 1999, 2001), and the effects of the transition from free convection to the stable regime (Nieuwstadt and Brost, 1986; Sorbjan, 1997; Acevedo and Fitzjarrald, 1999, 2001).

One ABL aspect that has not been fully investigated in terms of the LES technique relates to the effects of baroclinicity. Baroclinicity takes place when isobaric and isopycnic (constant density) surfaces intersect (e.g., Brunt, 1934). In the atmosphere, baroclinicity is caused by the presence of horizontal density gradients,

* E-mail: sorbjanz@mu.edu

Boundary-Layer Meteorology **112:** 57–80, 2004.

arising because of climatological contrasts in the north-south direction, and also because of thermal differences – evolving during the development of mesoscale weather systems, fronts, sea breezes – and due to slope and valley winds. The effects of baroclinicity can be demonstrated for the flow that is steady, geostrophic, and is in hydrostatic balance (Cushman-Roisin, 1994):

$$-fv = -(1/\rho_0)\ \partial p/\partial x, \tag{1a}$$

$$fu = -(1/\rho_0)\ \partial p/\partial y, \tag{1b}$$

$$\partial p/\partial z = -\rho g, \tag{1c}$$

where f is the Coriolis parameter ($f > 0$ in the Northern Hemisphere), p is the pressure, and ρ is the air density. By taking the z-derivative and eliminating the pressure we obtain:

$$\partial u/\partial z = [g/(\rho_0 f)]\partial\rho/\partial y, \tag{2a}$$

$$\partial v/\partial z = -g/(\rho_0 f)[\partial\rho/\partial x]. \tag{2b}$$

The obtained relations indicate that due to the Coriolis force, the system is maintained in equilibrium without the tendency toward levelling the density surfaces. The velocity field is not specified, only its vertical shear.

In the troposphere, an equatorial density gradient ($\partial\rho/\partial y > 0$) is expected to be accompanied by a positive geostrophic shear of the zonal flow ($\mathrm{d}u/\mathrm{d}z > 0$). As a result, motion becomes increasingly westerly with elevation. The density gradient, equivalent to a horizontal temperature gradient of 1 K per 100 kilometre, gives rise to a geostrophic wind shear as large as 3.5 m s^{-1} per kilometre. Therefore, westerlies, which intensify upward, can form subtropical jets (Salby, 1996). In the ABL, baroclinicity can significantly modify the thermal structure due to advection of cold or warm air, and also turbulence and mixing, due to baroclinic shear.

The thermal wind equations (2) are usually expressed in terms of the potential temperature Θ (Sorbjan, 1989):

$$\mathrm{d}u_g/\mathrm{d}z = -\beta/f\ \partial\Theta/\partial y, \tag{3a}$$

$$\mathrm{d}v_g/\mathrm{d}z = \beta/f\ \partial\Theta/\partial x, \tag{3b}$$

where u_g andv_g are the components of the geostrophic wind, $\beta = g/\Theta_0$ is the buoyancy parameter.

In the barotropic case, in which the temperature and geopotential surfaces are parallel and also horizontal, the horizontal temperature gradient is zero (Holton, 1972). Consequently, the geostrophic wind is independent of height. In the baroclinic case, the contours and isotherms intersect, and the horizontal temperature

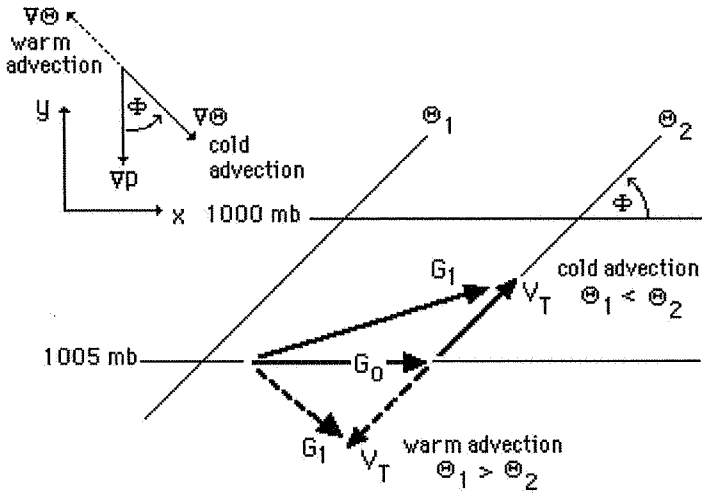

Figure 1. The baroclinic effects (in the Northern Hemisphere): the x-axis is oriented along the surface geostrophic wind vector G_0, G_1 is the geostrophic wind above the surface. The geostrophic wind turns with height to the right during warm advection, and to the left during cold advection. The termal wind $V_T = G_1 - G_0$ is parallel to isotherms, Θ is the angle between the horizontal pressure and temperature gradients.

gradient is non-zero (see Figure 1). When $\partial\Theta/\partial x > 0$, the geostrophic wind in the Northern Hemisphere turns with height to the left (so called backing,). This case will be referred here to as 'cold geostrophic advection' (C). When $\partial\Theta/\partial x < 0$, the geostrophic wind turns with height to the right (so called veering). This case is referred here to as 'warm geostrophic advection' (W). When $\partial\Theta/\partial x = 0$, and $\partial\Theta/\partial y < 0$, the geostrophic wind increases with height without changing its direction. We will refer to this case as the 'positive geostrophic shear' (PS). When $\partial\Theta/\partial x = 0$, and $\partial\Theta/\partial y > 0$, the geostrophic wind decreases with height without changing its direction. We will refer to this case as the 'negative geostrophic shear' (N). It should be stressed, that in the last two cases (P and N) there is no geostrophic advection of temperature, because contours and isotherms are parallel.

Baroclinic effects in the ABL were studied in the 1970s, based on empirical data and simple, one-dimensional models (Mahrt and Schwerdtfeger, 1970; Yordanov and Wippermann, 1972; Wippermann and Yordanov,1972; Wippermann, 1972; Wyngaard et al., 1974; Venkatesh and Csanady, 1974; Arya and Wyngaard, 1975). Such research was mostly performed in the context of the Rossby number similarity theory, or mixed layer modelling (Tennekes, 1980). There were a few attempts in the past to use LES in order to simulate the effects of geostrophic shear on the structure of the boundary layer (Brown, 1999). These were performed by imposing a vertical variation on the x-component of the geostrophic wind, and setting its y-component to zero. The isobaric and isopycnic surfaces in this case intersect in such a way that contours and isopycnics are parallel. This is equivalent to assuming pos-

itive or negative geostrophic shear with no heat advection. This special case is the simplest form of baroclinicity. It does not modify the thermal structure of the ABL, and therefore does not require modification of the LES equations. Other forms of baroclinicity require the adaptation of model equations in order to incorporate the thermal advection, with adjustment for the effects of buoyancy.

Despite much effort over a long period of time, baroclinic effects in the ABL have not been sufficiently understood, especially with respect to the turbulent structure of the mixed layer. Therefore, the purpose of this paper is to fully investigate the thermal and dynamical effects of baroclinicity in the dry, convective mixed layer, based on the large-eddy simulation model. Since statistical moments involving temperature are strongly sensitive in the mixed layer to thermal stratification in the free atmosphere (Sorbjan 1996b, c), it seems to be particularly interesting to examine a similar dependence on shear.

The paper is structured as follows. The LES model and the procedure required to include baroclinic effects are described in Section 2. The performed simulations are explained in Section 3, together with the results and the parameterization of the interfacial layer. Conclusions are given in Section 4.

2. The LES Model

The LES model developed by Sorbjan (1995, 2001) has been employed in this study. The model is based on a system of differential equations, consisting of conservation laws for momentum, mass, subgrid turbulent energy, and the first law of thermodynamics. The unknown quantities include three components of velocity, the virtual potential temperature, the specific humidity, the subgrid turbulent kinetic energy, and the pressure perturbations. The adopted sub-grid parametrization is based on the kinetic energy equation. The model applies a non-linear parametrization of the Reynolds stress (Kosovic and Curry, 1999), and a linear parametrization of scalar fluxes, with different eddy diffusivities in horizontal and vertical directions under stable conditions (Schumann, 1991). The multi-stage Runge–Kutta scheme is used for the time integration of all model equations. The time increment is adjusted on each time step based on the Courant–Friedrichs–Levy stability condition. The monotonic advection scheme is applied for scalar equations (Beets and Koren, 1996). The upper boundary conditions are assumed to be stress-free for horizontal velocity components, the vertical velocity is set to zero, and the potential temperature lapse rate is constant. The Monin–Obukhov similarity formulation is employed to calculate surface momentum fluxes on the first computational level.

In order to incorporate baroclinic effects into the model, the temperature and vertical velocity equations have been modified. The resolvable potential temperature Θ has been decomposed into the reference temperature Θ_r, and the local perturbation Θ'':

$$\Theta(x, y, z) = \Theta_r(x, y, z) + \Theta''(x, y, z). \tag{4}$$

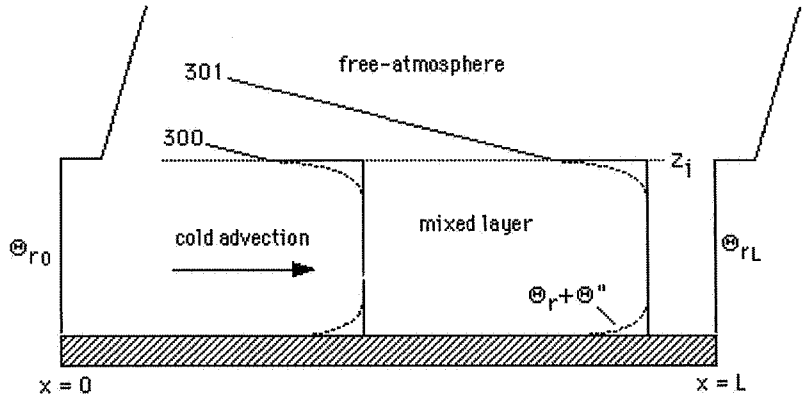

Figure 2. The isotherms in the baroclinic boundary layer during cold advection. The pressure gradient is assumed to be along the y-axis, which is perpendicular to the surface of the figure ($\partial p/\partial x = 0$, $\partial p/\partial y < 0$). The effects of local perturbation θ'' are indicated by broken lines. The dotted line marked by z_i indicates the top of the mixed layer. The values of the reference temperature at the beginning and at the end of the domain θ_{ro} and Θ_{rL} differ by $[L\ \partial\Theta_r/\partial x]$.

The reference temperature Θ_r is specified in the model. It varies along horizontal and vertical directions in the following way: $\Theta_r = \Theta_o + [\Delta\Theta + \Gamma(z - z_i)]I(z_i) + [x\ \partial\Theta_r/\partial x + y\ \partial\Theta_r/\partial y]$, where Θ_o is a constant, $I(z_i) = 0$ in the mixed layer (where $z < z_i$), and 1 above it, z_i is a specified depth of the mixed layer, $\Delta\Theta$ is the temperature jump at the top of the mixed layer, Γ is the temperature gradient in the free atmosphere. The components of the horizontal gradient $\partial\Theta_r/\partial x$ and $\partial\Theta_r/\partial y$ are assumed to be known constants.

The vertical structure of the baroclinic atmosphere, characterized by (4), is depicted in Figure 2. In the figure, the surfaces of constant potential temperature Θ are inclined in the free atmosphere, due to the presence of the horizontal temperature gradient. Heating and vigorous mixing in the mixed layer cause the temperature isosurfaces to turn toward the surface. The effects of the local perturbations Θ'' are marked by dotted lines. Note that the potential temperature Θ decreases with height in the surface layer, is constant with height in the mixed layer, and increases with height in the interfacial layer and in the free atmosphere.

It is convenient to rewrite (4) as

$$\Theta(x, y, z) = \theta(x, y, z) + [x\ \partial\Theta_r/\partial x + y\ \partial\Theta_r/\partial y], \tag{5}$$

where $\theta = \Theta'' + \Theta_o + [\Delta\Theta + \Gamma(z - z_i)]I(z_i)$ is the homogeneous contribution to the potential temperature, which obeys the periodic horizontal boundary conditions. It is treated as an unknown quantity in the described LES model. Based on Equation (5) the temperature equation in the model can be written in terms of θ (instead of Θ):

$$\begin{aligned} \partial\theta/\mathrm{d}t\ &+\ u\ \partial\theta/\partial x + v\ \partial\theta/\partial y + w\ \partial w\theta/\partial z + [u\ \partial\Theta_r/\partial x + v\ \partial\Theta_r/\partial y] \\ &=\ -\mathrm{div}\ H, \end{aligned} \tag{6}$$

TABLE I

Parameters of the simulated cases.

Run	Type	Φ	du_g/dz [10^{-3} s^{-1}]	dv_g/dz [10^{-3} s^{-1}]	w_* [m s^{-1}]	u_* [m s^{-1}]	z_i [m]	$-z_i/L$	T_s [s]
B	Barotropic	–	0	0	1.18	0.60	650	3.04	14718
P	Positive shear	0°	5	0	1.17	0.61	632	2.83	10293
C	Cold advection	90°	0	5	1.17	0.69	635	1.95	14467
N	Negative shear	180°	−5	0	1.17	0.60	637	3.03	16168
W	Warm advection	270°	0	−5	1.18	0.54	644	4.17	14660

where u, v, w are the components of the wind velocity, the term on the right-hand-side is the heat flux vector divergence, $H = -k_h \text{ grad } \theta$, and k_h is the eddy diffusivity. The contributions of $\partial\Theta_r/\partial x$ and $\partial\Theta_r/\partial y$ on the right-hand side of (6) are neglected. Based on (3), the last term on the left-hand side of (6) is prescribed as geostrophic advection:

$$[u\,\partial\Theta_r/\partial x + v\,\partial\Theta_r/\partial y] \approx -(f/\beta)[u_g\,dv_g/dz - v_g\,du_g/dz]. \tag{7}$$

The buoyancy term in the third momentum equation is expressed in terms of θ:

$$\beta[\Theta - \Theta_o] \approx \beta[\theta - \langle\theta\rangle]. \tag{8}$$

3. The Results

3.1. THE LES EXPERIMENTS

The characteristics of the performed simulations are summarized in Table I. Here, u_g and v_g are the components of the geostrophic wind, z_i is the mixed layer height, $w_* = (\beta H_o z_i)^{1/3}$ is the convective velocity scale, H_o is the surface temperature flux, β is the buoyancy parameter, u_* is the friction velocity, L is the Obukhov length, $-z_i/L$ is the stability parameter, and T_s is the time length of a simulation. Five runs of the model are presented: one barotropic (B), and four baroclinic – for four different values of the angle Φ between the isobars and isotherms, as depicted in Figure 1. The simulated cases are: the negative and the positive geostrophic shear cases (P, and N), for which $\Phi = 0°$ and 180° respectively, and also the cold and warm advection cases (C and W), with $\Phi = 90°$ and 270°.

It should be noted that similar cases of geostrophic shear were considered by Brown (1996). His simulations, however, cannot be considered baroclinic, because as applied by him geostrophic shear is not related to the temperature field. The

temperature in his LES model is assumed periodic in horizontal directions (for all combinations of geostrophic shear). Consequently, there is no temperature advection. Moreover, his mixed layer is capped by a solid lid, so there is no entainment, and the heat flux at the top is set to zero. Such a turbulent flow does not seem to have an analogue in the atmospheric boundary layer.

All five simulations considered in this paper employed a mesh with $64 \times 64 \times 60$ grid points, and with grid increments of $\Delta x = \Delta y = 40$ m, and $\Delta z = 30$ m. The geostrophic wind at the earth's surface was the same in all runs, equal to $G_0 = 15$ m s^{-1}. The components of the geostrophic wind in the baroclinic cases varied by 5 m s^{-1} per kilometre. The roughness parameter was set to $z_o = 0.01$ m, the surface kinematic heat flux $H_o = 0.075$ m K s^{-1}, and the Coriolis parameter $f = 10^{-4}$ s^{-1}. The model was initialised assuming that the initial mixed layer height equals $z_i = 600$ m, with a potential temperature of 299 K. The interfacial layer above the mixed layer was 150 m thick, with the vertical temperature gradient $\gamma = 30$ K km^{-1}. In the free atmosphere the vertical temperature gradient was assumed to be $\Gamma = 3$ K km^{-1}.

All simulations were run for 10,200 time steps. Because the time increments during all simulations were automatically adjusted on each time step (based on the Courant–Friedrichs–Levy stability condition), the simulation time T_s in Table I is different for each run. This fact did not introduce any difficulties in the interpretation of the final results. Due to the strong temperature gradient at the top of the mixed layer, and a constant heat flux at the surface, all characteristics of turbulence, including the mixed layer height z_i, differed little from each other. The statistics presented in this paper were obtained through the horizontal and temporal averaging during the last 1200 time steps of each simulation, which is equivalent to about 1000–1200 sec, or approximately to two overturning time scales, defined as $\tau_c = z_i/w_*$.

Figure 3 shows the time history of the mixed layer height z_i, and the ratio of the heat fluxes $R = H_i/H_o$ at the top and bottom of the mixed layer during the barotropic simulation (B). The oscillations that appear in the first part of the simulation are numerical in origin, and disappear after about 10,000 sec. The short oscillations have a period comparable with the convective time scale $\tau_c = z_i/w_* \approx 600$ sec, which can be associated with the frequency of rising thermals.

3.2. THE VELOCITY MOMENTS

The u and v wind components are shown in Figure 4, which indicates that there is a sharp increase of velocity in the surface layer, from zero at the earth's surface, to the mixed layer values, reached at about $z/z_i = 0.25$. In the mixed layer, the wind velocity is approximately constant, up to about $z/z_i = 0.75$. From this level, up to about $z/z_i = 1.25$, where the free atmosphere values of the geostrophic wind are attained, there is a strong variation in wind speed.

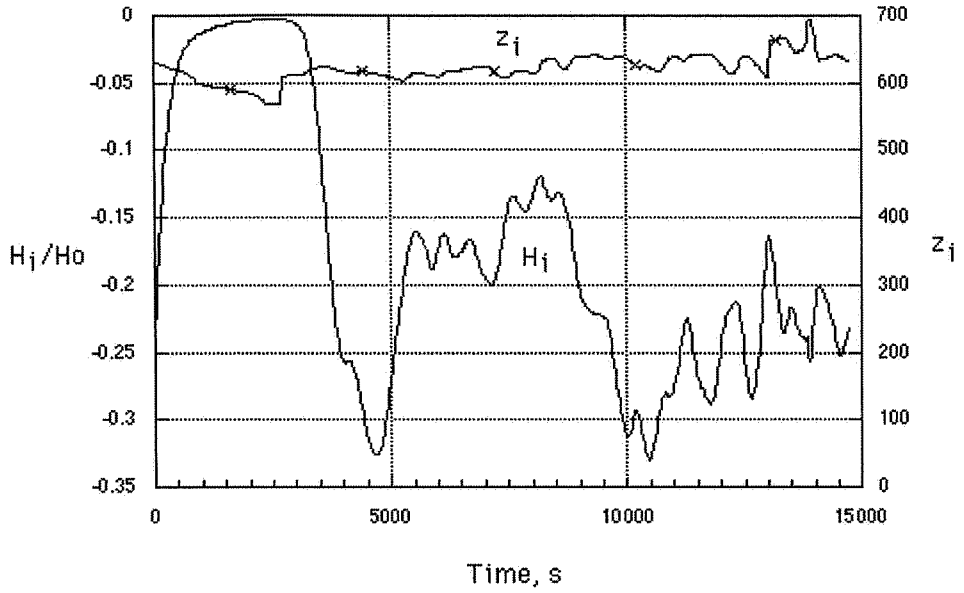

Figure 3. The time history (plotted every 20 time steps) of the mixed-layer height z_i (the right scale) and the ratio of the heat flux values H_i/H_o at the top and the bottom of the mixed layer (the left scale) during the barotropic simulation (B).

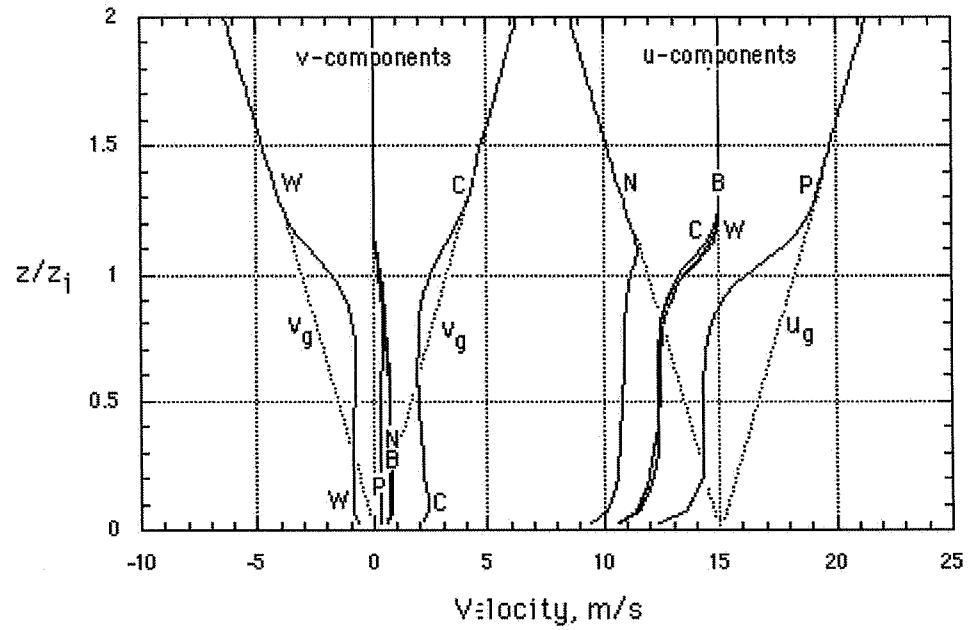

Figure 4. Profiles of the u (on the right) and v (on the left) components of wind velocity, obtained for five runs: B – barotropic case, W – warm advection, C – cold advection, P – positive shear, N – negative shear. The components of the geostrophic wind are indicated by dotted lines.

During both warm and cold geostrophic advection (W, C), the u component of wind coincides with those during the barotropic advection (B). Note that the x-component of the geostrophic wind in these three cases is constant with height, and equal to 15 m s^{-1}. The u component of wind increases from zero at the earth's surface to about 12.5 m s^{-1} in the mixed layer, which is about 83% of the geostrophic wind velocity. For comparison, Moeng and Sullivan (1994) obtained a 75% reduction of wind in the mixed layer, when the geostrophic wind was 10 m s^{-1}. There is a sharp increase of u above the mixed layer, equal to about 2.5 m s^{-1}.

In the case of a positive geostrophic shear (PS), the u component of the geostrophic wind (u_g) increases by 5 m s^{-1} per kilometre. In the mixed layer, the u component of the wind velocity is equal to 14.3 m s^{-1}, which is about 85% of the mean geostrophic wind velocity in the mixed layer (i.e., 16.7 m s^{-1} at $z = z_i/2$). The sharp increase of u above the mixed layer is equal to about 5 m s^{-1} (from about 14.3 m s^{-1} to about 19.3 m s^{-1}).

In the case of a negative geostrophic shear (N), u_g decreases by 5 m s^{-1} per kilometre. The u component of wind velocity in the mixed layer is equal to about 11 m s^{-1}, which is about 81% of the mean geostrophic wind velocity in the mixed layer (equal to 13.5 m s^{-1}). There is a small increase of u above the mixed layer, equal to about 1 m s^{-1}. The interfacial layer seems to be thinner than in all the cases discussed above.

During cold geostrophic advection (C), the v component of wind is positive and increases with height, following the increase of v_g (which is 5 m s^{-1} per kilometre). During warm geostrophic advection (W), the v component of wind velocity is negative and decreases with height, following v_g, which decreases with height.

The v components of wind velocity in both cases, C and W, are of different signs. They are not symmetrical, due to the effects of the Coriolis force. In the Northern Hemisphere, the Coriolis force causes a small (in convective conditions), positive (left) cross-isobar angle. As a result, the v component is slightly larger during cold advection than during warm advection. In the barotropic case, and also during positive and negative shear cases (P and N), the v components of wind velocity are positive.

The profiles of the momentum fluxes are shown in Figure 5. The fluxes are scaled in terms of w_*^2. In the mixed layer, all the x components of the momentum flux are linear. Near the earth's surface, they are negative, because the momentum fluxes in this region are expected to have opposite signs to gradients of du/dz, which are positive in the surface layer. The same rule applies at the top of the mixed layer, where all the x components of the momentum flux are also negative, as $du/dz > 0$ at this level.

All of the y components of the momentum flux near the earth's surface are negative, except in the W case (this is because in this case $dv/dz < 0$ in the surface layer, see Figure 4). At the top of the mixed layer, the y components of the momentum flux have different signs. They are positive during B, W and N

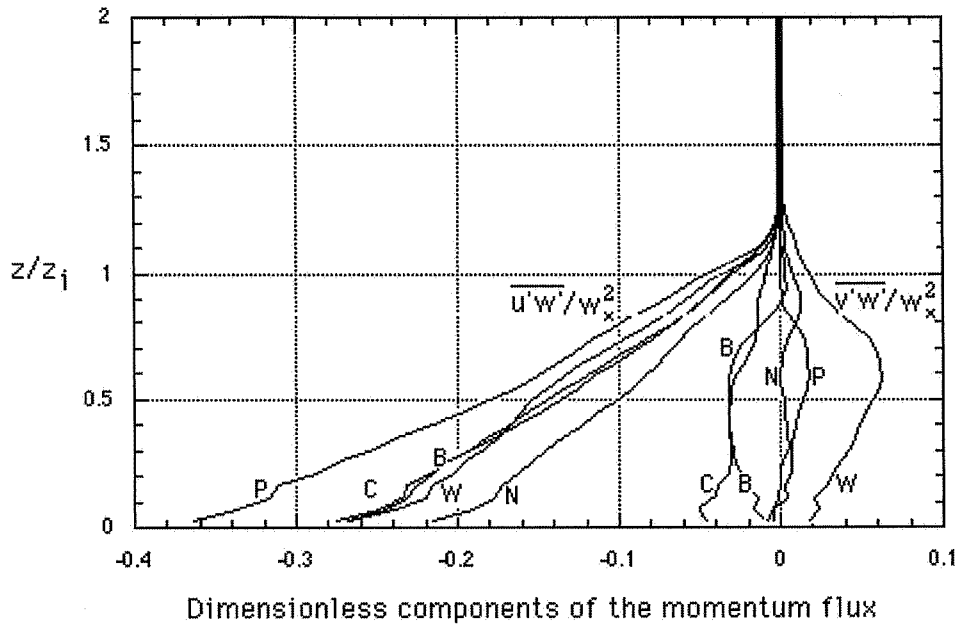

Figure 5. Profiles of the dimensionless momentum flux (scaled by w_*^2) for five runs: B – barotropic case, W – warm advection, C – cold advection, P – positive shear, N – negative shear.

cases, as $dv/dz > 0$ near $z = z_i$ in these cases. The y component for C is negative at $z = z_i$, because $dv/dz > 0$ at this height. In the P case, the y component of the momentum flux is near zero at the top of the mixed layer, because dv/dz is small in this region, as seen in Figure 4.

The profiles of the dimensionless horizontal velocity variance σ_u^2/w_*^2 are shown in Figure 6. The variances sharply decrease with height in the lower half of the mixed layer, and are nearly constant or slightly increasing functions of height in the upper half. At $z = z_i$, pronounced differences can be seen among variance values. The largest value of σ_u^2/w_*^2 is obtained for the P curve, and the smallest for the N curve. It could be noted that profiles of the dimensionless horizontal velocity variance σ_v^2/w_*^2 (not shown) are almost the same for all cases, and similar to profile B in Figure 6.

The profiles of the dimensionless vertical velocity variance σ_w^2/w_*^2 are shown in Figure 7. In the mixed layer, the variances are nearly the same for all cases. They increase in the lower half of the mixed layer, reach maxima, and gradually decrease with height. More pronounced differences can be seen in the interfacial layer. These differences are induced by the effects of shear on the top of the mixed layer, and will be further discussed in Section 4.

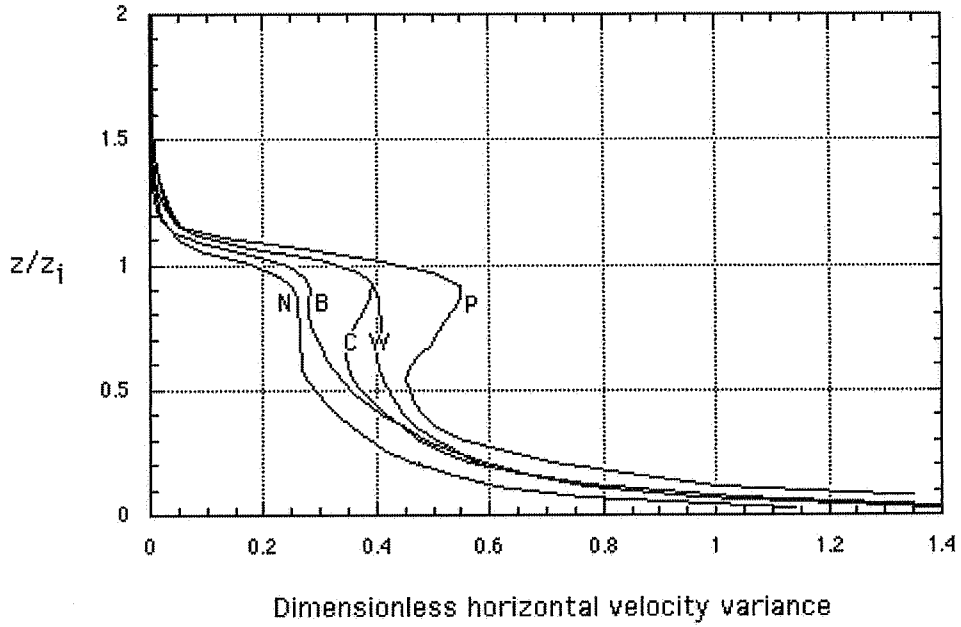

Figure 6. Profiles of the dimensionless horizontal velocity variance (scaled by w_*^2) for five runs: B – barotropic case, W – warm advection, C – cold advection, P – positive shear, N – negative shear.

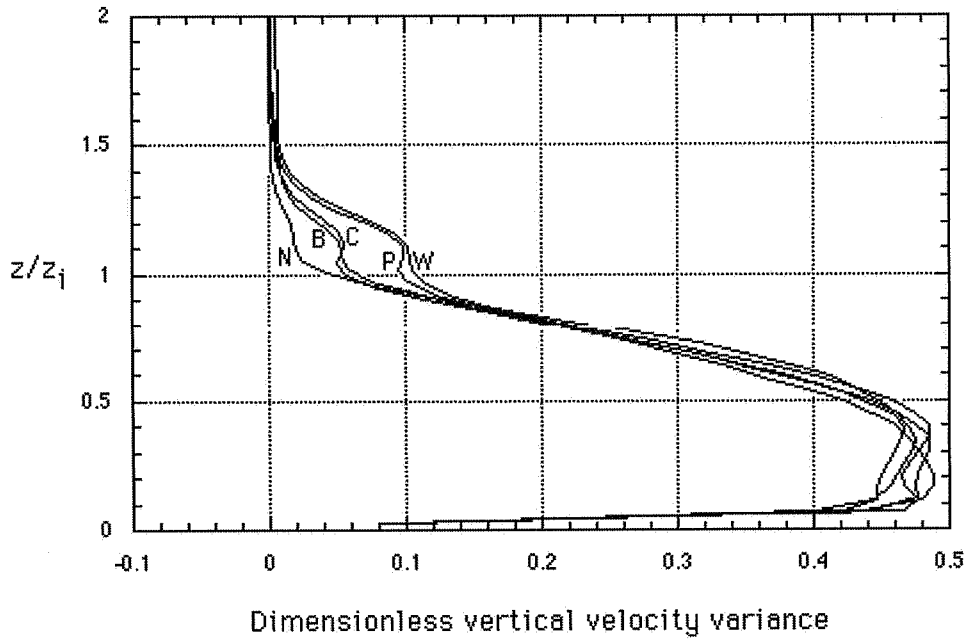

Figure 7. Profiles of the dimensionless vertical velocity variance (scaled by w_*^2) for five runs: B – barotropic case, W – warm advection, C – cold advection, P – positive shear, N – negative shear.

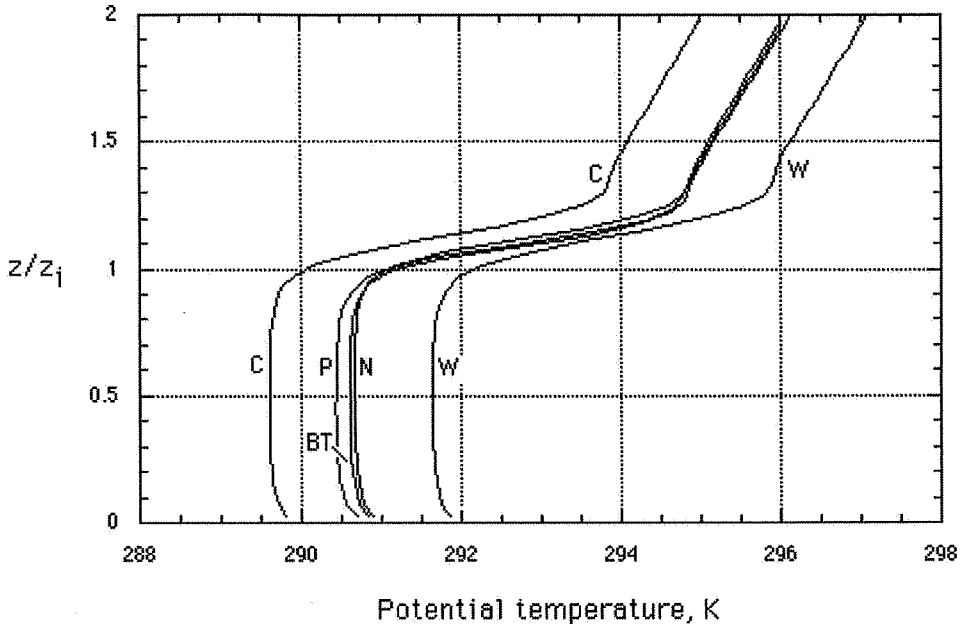

Figure 8. Profiles of the potential temperature for five runs: B – barotropic case, W – warm advection, C – cold advection, P – positive shear, N – negative shear.

3.3. THE TEMPERATURE MOMENTS

The potential temperature profiles obtained for all five simulations are shown in Figure 8. Since the initial potential temperature in the mixed layer was equal to 290 K, the advective effects, or their lack, are quite obvious. In the B, P, and N simulations with no geostrophic advection, the turbulent warming is exclusively due to the positive heat flux at the surface and due to entrainment. This causes the mixed layer temperature to increase less than 1 K during each simulation. Small differences in heating rates in the mixed layer among the runs B, P, N can be explained by different time lengths T_s in each simulation, depicted in Table I (T_s is the largest for N, and the smallest for P). Larger heating and cooling during the W and C runs are due to advective effects. The obtained profiles of the potential temperature in these cases are similar to those observed in the atmosphere (Sorbjan, 1996a; LeMone et al., 2000).

The profiles of the dimensionless temperature flux are shown in Figure 9. All the flux profiles are linear, but have different values of H_i at the top of the mixed layer. The flux H_i is the largest in the P run, and the smallest in the N run. This result is explained in the next Section.

The dimensionless temperature variances are shown in Figure 10. The variances are scaled in terms of the convective temperature scale $\Theta_* = H_o/w_*$, and are large at the earth's surface, reaching minimum values at roughly $z/z_i = 0.7$. Above the

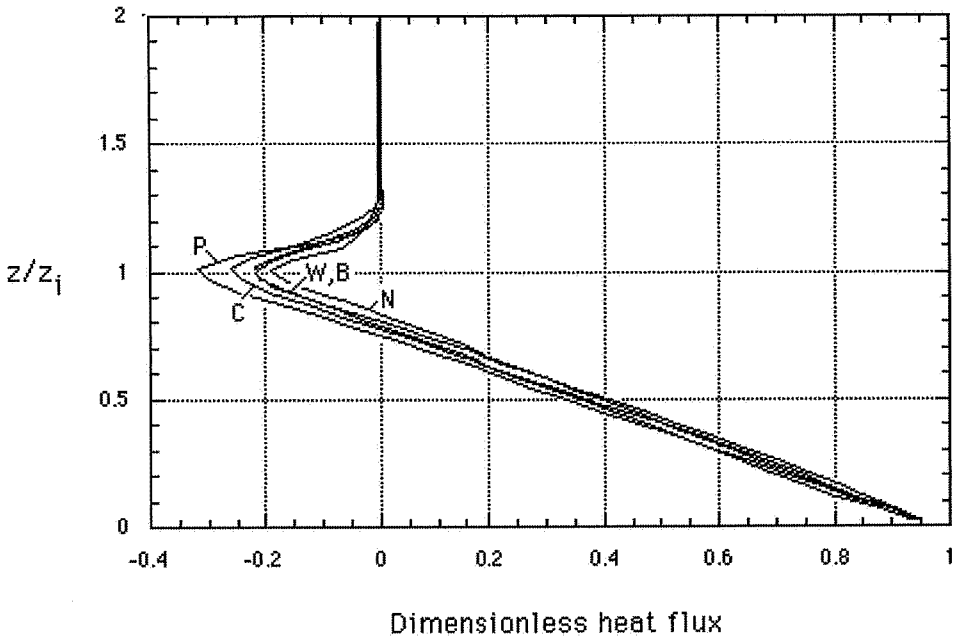

Figure 9. Profiles of the dimensionless potential temperature flux for five runs: B – barotropic case, W – warm advection, C – cold advection, P – positive shear, N – negative shear.

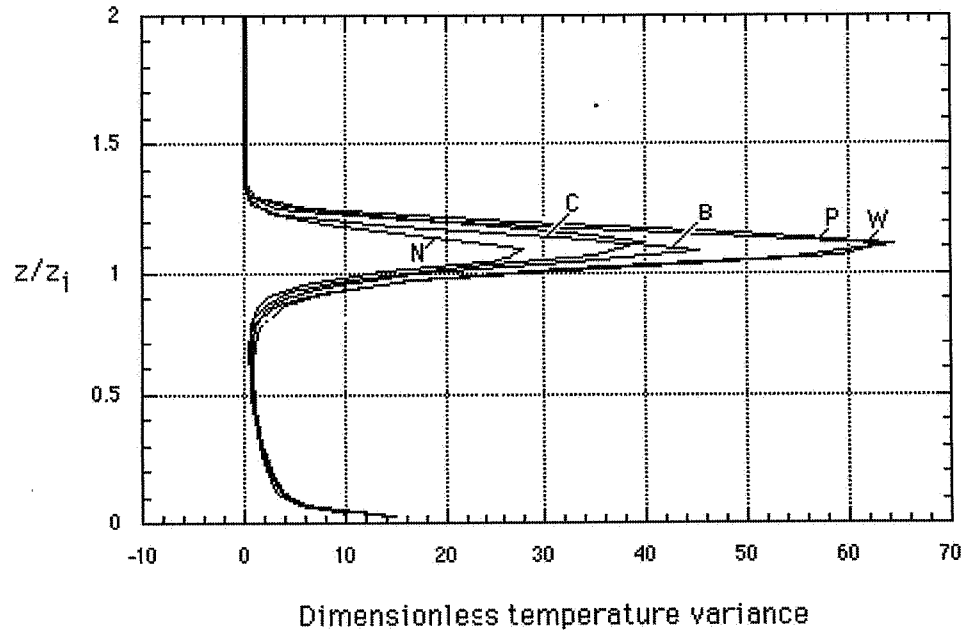

Figure 10. Profiles of the dimensionless potential temperature variance (scaled by w_*^2) for five runs: B – barotropic case, W – warm advection, C – cold advection, P – positive shear, N – negative shear.

TABLE II

Characteristics of the interfacial layer in the simulated cases

Run	du_g/dz [10^{-3} s^{-1}]	dv_g/dz [10^{-3} s^{-1}]	du/dz [10^{-3} s^{-1}]	dv/dz [10^{-3} s^{-1}]	$d\Theta/dz$ [10^{-3} K m^{-1}]	Ri	h [m]
BT	0	0	11.5	−1.9	24.5	5.91	163
PS	5	0	17.7	1.0	25.2	2.64	159
NS	−5	0	1.9	−1.9	24.8	109.15	161
WA	0	−5	15.7	−12.6	25.2	2.05	159
CA	0	5	9.9	5.9	25.3	6.29	158

mixed layer, the profiles reach maxima, at about $z/z_i = 1.1$. The maximum values are the largest in the P run and the smallest in the N run. The differences are caused by the impact of shear and entrainment, and will be explained in the next Section.

3.4. THE INTERFACIAL LAYER

In this section, the focus will be directed to the structure of the interfacial layer, where turbulence, controlled by wind shear and buoyancy, gradually vanishes with height. Three characteristics of turbulence of the interfacial layer will be considered, i.e., the vertical velocity variance σ_w^2, the temperature variance σ_θ^2, and the temperature flux H. The selected moments, evaluated at the top of the simulated mixed layer, will be related to vertical gradients of velocity and temperature in the interfacial layer.

The characteristics of the simulated interfacial layer are displayed in Table II. In the Table, du_g/dz and dv_g/dz are the components of the vertical geostrophic shear, du/dz and dv/dz are the gradients of velocity components in the interfacial layer, $d\Theta/dz$ is the potential temperature gradient in the interfacial layer, Ri is the interfacial layer Richardson number, defined as $\mathrm{Ri} = (\beta\, d\Theta/dz)/[(dv/dz)^2 + (dv/dz)^2]$, and h is the height of the interfacial layer. The values of h, depicted in the Table, were evaluated from the potential temperature profiles, by approximating the profiles as three straight lines (in the mixed layer, in the interfacial layer and in the free atmosphere). The values obtained in this way coincide with the values of h calculated based on profiles of the heat flux, as a difference between points, where the heat flux decreases to zero and where the heat flux is minimum.

First to be discussed is the simplified budget of the turbulent kinetic energy at the top of the mixed layer. It includes a steady-state balance of the dissipation rate, turbulent transport, shear production, and buoyant production terms (the pressure term has been neglected):

$$E_i^{3/2}/l_i = TT_i + k_{mi}[(du/dz)^2 + (dv/dz)^2]_i + \beta H_i, \tag{9}$$

where the term on the left-hand side expresses the dissipation rate, TT is the turbulent transport term, the last two terms are shear production and buoyant production, respectively. In the above equation, E is the turbulent kinetic energy, l is a mixing length, k_m is the eddy viscosity, β is the buoyancy parameter, H is the temperature flux, and the index 'i' indicates that all values are calculated at $z = z_i$.

Assuming that at the top of the mixed layer the turbulent transport and shear production terms are proportional (see e.g., Figure 1 in Sorbjan, 2001), and that also $k_{mi} \sim l_i E_i^{1/2}$, $E_i \approx \sigma_{wi}^2 \approx w_*^2$, $l_i \approx h$, where h is the height of the interfacial layer, and $H_i \approx -H_o$, we obtain:

$$\sigma_{wi}^2 = c_w w_*^2 + c_h h^2 (s_{xi}^2 + s_{yi}^2), \tag{10}$$

where c_w and c_h are constants, and $s_x = \mathrm{d}u/\mathrm{d}z$, $s_y = \mathrm{d}v/\mathrm{d}z$. The height of the interfacial layer in (10) can be evaluated by assuming that the turbulent kinetic energy of a thermal is lost within this layer as work against the buoyancy force, i.e., $w_*^2 \approx \beta \gamma_i^2$, where γ_i is the temperature gradient in the interfacial layer. From this we have:

$$h \sim w_*/(\beta \gamma_i)^{1/2}. \tag{11}$$

Note that the obtained formula can be expressed in terms of the bulk Richardson number, defined as $\mathrm{Ri}_B = \beta \Delta\Theta \, z_i / w_*^2$, where $\Delta\Theta$ is the temperature jump at the top of the mixed layer. Since $\gamma_i \sim \Delta\Theta/h \sim \beta \, \Delta\Theta^2/w_*^2$, $(\beta\gamma_i)^{1/2} \sim \beta \Delta\Theta / w_*$, therefore $h/z_i \sim w_*/[z_i(\beta\gamma_i)^{1/2}] \sim \mathrm{Ri}_B^{-1}$. This coincides with Deardorff et al. (1980), who suggested that $h/z_i \approx a_1 + a_2/\mathrm{Ri}_B$, where a_1 and a_2 are constants.

Based on (11), Equation (10) can be rewritten in the following form:

$$\sigma_{wi}^2 = c_w w_*^2 [1 + c_s (s_{xi}^2 + s_{yi}^2)/(\beta \gamma_i)]. \tag{12}$$

The constant c_w can be interpreted as the value of the dimensionless vertical velocity variance during shearless convection. For the specific values $c_w = 0.05$ and $c_s = 1.8$, and the values of the gradients s_{xi}, s_{yi} and γ_i from Table II, Equation (12) is examined in Figure 11. This indicates that Equation (12) approximates the LES results quite well.

In order to relate the temperature flux and the temperature variance to the characteristics of the interfacial layer, we employ the local similarity theory of type II, proposed by Sorbjan (2001). The theory uses scales based on the local values of scalar gradients at the top of the mixed layer, instead of scales based on fluxes (which were applied by Nieuwstadt (1984), and also by Sorbjan (1995), within local similarity theory, referred to here as type I).

According to Sorbjan (2001), when the effects of wind shear dominate, turbulence is expected to be characterized by the following set of local scales for vertical velocity, length and potential temperature respectively:

$$U_T = \sigma_w, \tag{13a}$$

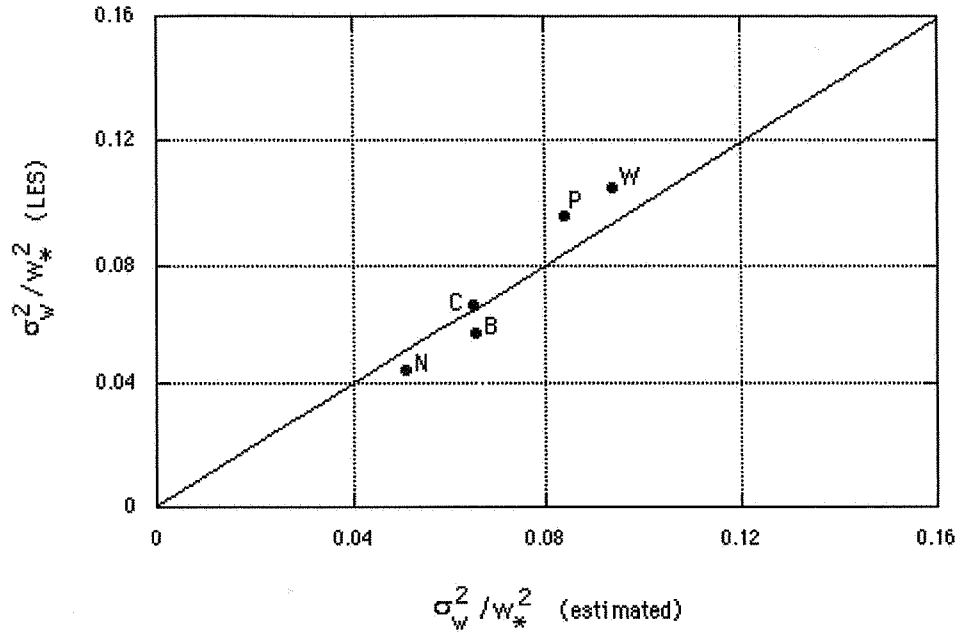

Figure 11. Comparison of the vertical velocity variance at the top of the mixed layer obtained from the LES model with its estimated value based on Equation (12). B – barotropic case, W – warm advection, C – cold advection, P – positive shear, N – negative shear.

$$\Lambda_T = \sigma_w/(s_x^2 + s_y^2)^{1/2}, \tag{13b}$$

$$\Theta_T = \Lambda_T \gamma, \tag{13c}$$

where γ and s_x, s_y are the vertical gradients of the potential temperature and wind velocity components, and σ_w^2 is the vertical velocity variance. Based on these local scales, the following predictions for the heat flux H and temperature variance σ_θ^2 can be obtained within the interfacial layer:

$$H \sim U_T \Theta_T \sim \sigma_w^2 \gamma/(s_x^2 + s_y^2)^{1/2}, \tag{14}$$

$$\sigma_\theta^2 \sim \Theta_T^2 \sim \sigma_w^2 \gamma^2/(s_x^2 + s_y^2). \tag{15}$$

In the shearless case (when there is no mean wind), local similarity implies the following local scales (Sorbjan, 2001):

$$U_B = \sigma_w, \tag{16a}$$

$$\Lambda_B = \sigma_w/(\beta\gamma)^{1/2}, \tag{16b}$$

$$\Theta_B = \Lambda_B \gamma. \tag{16c}$$

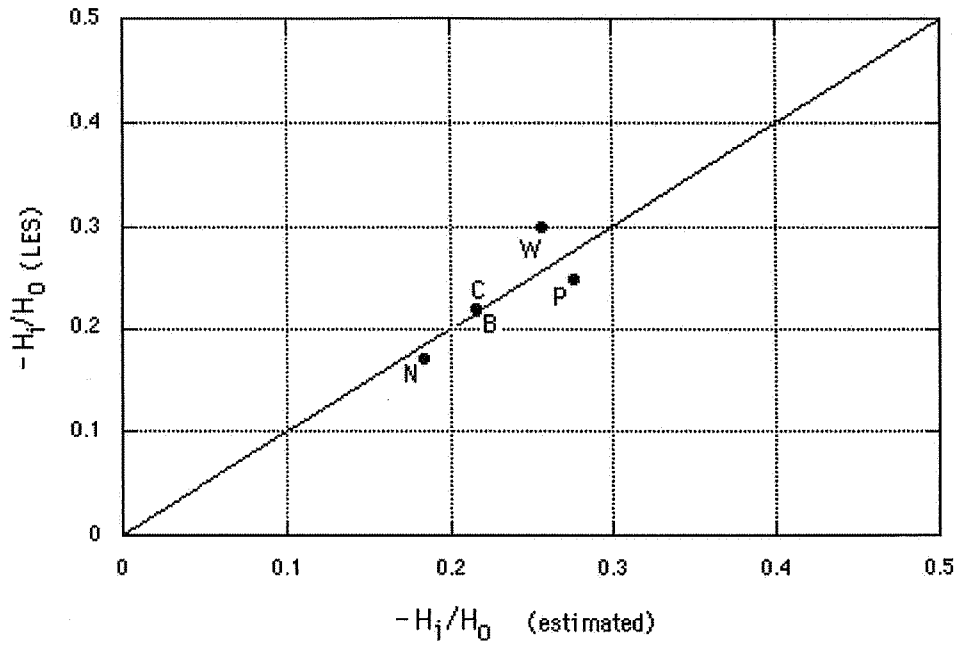

Figure 12. Comparison of the temperature flux ratio $-H_i/H_o$, obtained from the LES model, with its estimation based on Equation (19), B – barotropic case, W – warm advection, C – cold advection, P – positive shear, N – negative shear.

From this, the following predictions for the temperature flux H, and temperature variance σ_θ^2 are obtained within the interfacial layer:

$$H \sim U_B \Theta_B \sim \sigma_w^2 \gamma / (\beta\gamma)^{1/2}, \tag{17}$$

$$\sigma_\theta^2 \sim \Theta_B^2 \sim \sigma_w^2 \gamma^2 / (\beta\gamma). \tag{18}$$

When both the wind and temperature stratifications are equally significant, one might propose expressions that asymptotically coincide with Equations (14), (15) and (17), (18):

$$H_i = C_1 \sigma_{wi}^2 \gamma_i / (s_{xi}^2 + s_{yi}^2 + \beta\gamma_i)^{1/2}, \tag{19}$$

$$\sigma_{\theta m}^2 = C_2 \sigma_{wi}^2 \gamma_i^2 / (s_{xi}^2 + s_{yi}^2 + \beta\gamma_i), \tag{20}$$

where the index 'i' indicates the level at $z = z_i$. Note that the temperature variance $\sigma_{\theta m}^2$ is not calculated at $z = z_i$, but at the level of its peak, which appears at $z/z_i = 1.1$ (see Figure 8). The expressions (19) and (20) are valid for all values of s_{xi} and s_{yi} and for $\gamma_i > 0$.

Inspection of Equations (19) and (20) indicates that both moments are dependent on the temperature gradient γ_i in the interfacial layer. As pointed out

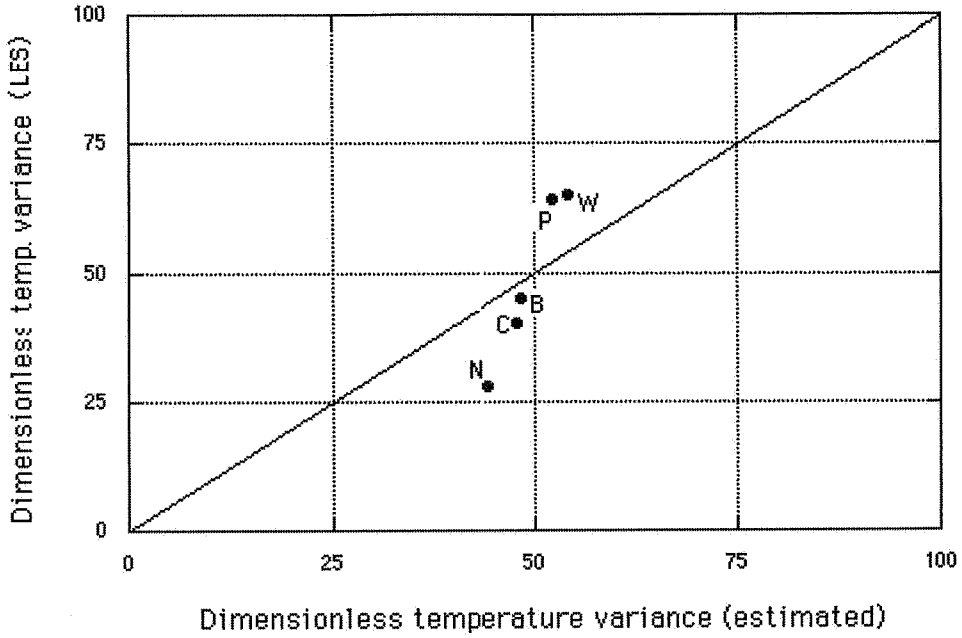

Figure 13. Comparison of the dimensionless peak value of the temperature variance, obtained from the LES model, with its estimation based on Equation (20). B – barotropic case, W – warm advection, C – cold advection, P – positive shear, N – negative shear.

by (Sorbjan, 1996b, c) this dependence is expected and especially evident during an early morning transition, called 'free encroachment'. Free encroachment takes place when the mixed layer begins to grow into a neutrally stratified layer ($\gamma_i = 0$) – the residual of the previous day's well-mixed layer. This growth occurs approximately with the speed of rising updrafts. As a result, the entrained air does not differ thermally from the air in the mixed layer, which causes the heat flux and the temperature variance at the top of the mixed layer to vanish.

Based on the performed simulations, we found that $C_1 = -0.15$ and $C_2 = 1.5$. For these values and for the velocity variance calculated based on (12), Equations (19) and (20) are compared in Figures 12 and 13 with the LES results. The Figures indicate that the performance of Equation (19) is good, but that of Equation (20) seems to be poorer.

Equation (19) should be compared with the relation for the heat flux ratio: $R = -H_i/H_o = [0.2 + A(u_*/w_*)^3]$, which has been commonly used in models to express the effects of shear within the mixed layer. According to Tennekes (1973), Driedronks (1982), and Moeng and Sullivan (1994), the constant A is about 5. It can be noted, that contrary to (19), the above formula does not reflect the impact of thermal stratification in the free atmosphere. For the LES values of u_* and w_* shown in Table I, the above formula gives values of the heat flux ratio R in the

range 0.68–1.23. These values overestimate the LES values of R, which according to Figure 11, are in the range 0.17–0.3.

In the shearless ABL, Equations (12), (19), and (20) can be rewritten as:

$$\sigma_{wi}^2 = c_w w_*^2, \tag{21a}$$

$$H_i = c_H \, w_*^2 N_i/\beta, \tag{21b}$$

$$\sigma_{\theta m}^2 = c_\theta \, w_*^2 N_I^2/\beta^2, \tag{21c}$$

where $N_i = [\beta\gamma_i]^{0.5}$ is the Brunt–Väisäla frequency in the interfacial layer, $c_H = c_w C_1$, and $c_\theta = c_w C_2$. It is worth mentioning that Equation (21b) can also be derived based on the simplified equations for temperature flux and temperature variance (in which only the production and dissipation terms are retained, and the time scale is assumed to be inversely proportional to the Brunt–Väisäla frequency N – see Equation (2) by Sorbjan (1996c). The vertical velocity variance σ_{wi}^2 in (21) is independent of N, which agrees with a similar conclusions of Sorbjan (1996c). In the free-encroachment case, when $N = 0$, the correct asymptotes are obtained: $H_i = 0$, and $\sigma_{\theta m} = 0$.

The forms of Equation (21) indicate that the following expressions can be adopted as interfacial scales:

$$S_\theta = w_* N_i/\beta, \tag{22a}$$

for temperature,

$$S_w = w_*, \tag{22b}$$

for vertical velocity,

$$S_h = w_*/N_i, \tag{22c}$$

for height,

$$S_t = 1/N_i, \tag{22d}$$

for time.

The above scales are related to values of the surface heat flux through the convective scale $w_* = (\beta H_o z_i)^{1/3}$, and to the interfacial layer stratification through the Brunt–Väisäla frequency $N_i = [\beta\gamma_i]^{0.5}$. For $H_o = 0.05$ K m s^{-1}, $z_i = 700$ m, $\gamma_i = 30$ K km^{-1}, we have $S_w \approx w_* \approx 1$ m s^{-1}, $S_\theta \approx 1$ K, $S_h \approx 30$ m, $S_t \approx 30$ s.

In terms of interfacial scales, dimensionless moments at the top of the shearless mixed layer are expected to be universal constants. For this reason, the interfacial scaling is expected to perform better in the interfacial region than convective scaling, proposed by Deardorff (1970a, b). Convective scaling (z_i, w_*, and Θ_* as the

height, velocity, and temperature scales) have been known to yield a substantial scatter of dimensionless quantities at the top of the mixed layer (Sorbjan, 1991, 1999). This fact was explained by Sorbjan (1996b, c), who found that the statistical moments involving temperature are strongly sensitive to the variation of the potential temperature gradient in the free atmosphere.

In order to apply (21) in practice, one might rewrite (11) in the form $\gamma_i \sim \Delta\Theta/h \sim \beta\,\Delta\Theta^2/w_*^2$, where $\Delta\Theta$ is the temperature jump at the top of the mixed layer, and use the time rate equation to calculate $\Delta\Theta$: $\mathrm{d}(\Delta\Theta)/\mathrm{dt} = \Gamma\,\mathrm{d}z_i/\mathrm{dt} - (H_i - H_o)/z_i$, where Γ is the vertical temperature gradient in the free atmosphere. The growth of the mixed layer could be additionally evaluated by assuming that $\mathrm{d}z_i/\mathrm{dt} \sim h/\tau_c$, where the mixed-layer time scale $\tau_c = z_i/w_*$. This yields: $\mathrm{d}z_i/\mathrm{dt} \sim H_o/\Delta\Theta$, which agrees with the laboratory result of Deardorff et al. (1980), and also with LES experiments. Rewritting this expression in the form: $\Delta\Theta\,\mathrm{d}z_i/\mathrm{dt} \sim H_o$, and comparing it with the expression derived by Lilly (1968), according to which $\Delta\Theta\,\mathrm{d}z_i/\mathrm{dt} = -H_i$, we see that Lilly's formula is inconsistent with the presented parameterization, because it leads to a conclusion $H_i/H_o \sim$ constant, which is contradictory to Equation (21).

Finally, when shear is present in the atmosphere, Equations (12), (19), and (20) can be rewrittten in the following form:

$$\sigma_{wi}^2 = c_w w_*^2(1 + c_2/\mathrm{Ri}), \tag{23a}$$

$$H_i = c_H w_*^2(N_i/\beta)(1 + c_2/\mathrm{Ri})/(1 + 1/\mathrm{Ri})^{1/2}, \tag{23b}$$

$$\sigma_{\theta m}^2 = c_\theta w_*^2(N_i^2/\beta^2)(1 + c_2/\mathrm{Ri})/(1 + 1/\mathrm{Ri}), \tag{23c}$$

where Ri is the interfacial Richardson number, $\mathrm{Ri} = \beta\gamma_i/(S_{xi}^2 + S_{yi}^2)$.

The obtained result suggests that the dimensionless moments at the top of the mixed layer, with shear, are not universal constants, as in the shearless case, but are functions of the Richardson number. This conclusion agrees with the analysis by Sorbjan (2001). Note that, when $\mathrm{Ri} \to \infty$ (the shearless case), $\mathrm{Ri}^{-1} \to 0$, and the dependence on Ri vanishes in (23).

4. Conclusions

The simultaneous effects of shear and buoyancy in the dry and baroclinic mixed layer have been examined based on the large-eddy simulations. The obtained results show that baroclinicity modifies not only the vertical distribution of temperature and wind in the boundary layer, but also affects the second-order statistics of turbulence.

Based on the performed simulations, a new parametrization of the interfacial layer has been developed. It employs the interfacial scaling, based on the Brunt-Väisälä frequency N in the interfacial layer, convective scale w_*, and the buoyancy

parameter β. In terms of this scaling, the dimensionless statistical moments at the top of the shearless mixed layer are expected to be universal constants. In the mixed layer with shear, the dimensionless statistical moments at the top of the mixed layer are expected to be functions of the interfacial Richardson number.

The interfacial scaling differs from the convective scaling introduced by Deardorff. This fact implies the presence of two different regimes in the mixed layer. The first, in the core part of the mixed layer, is controlled by surface heating, and can be described by Deardorff's scales. The second one is controlled by thermal stratification and shear in the interfacial layer, and requires the interfacial scaling.

The presence of these two different regimes makes formulating a general similarity theory for the mixed layer difficult. Nevertheless, one might expect that similarity functions should be written as a sum of two components. The first one should be expressed in terms of Deardorff's scaling, and should coincide with the Monin–Obukhov predictions in the surface layer. The second one should be expressed in terms of the interfacial scales, and the interfacial Richardson number Ri in the sheared case.

References

Acevedo, O. and Fitzjarrald, D. R.: 1999, 'Observational and Numerical Study of Turbulence during Early Evening Transition', in *13th Symposium on Boundary Layers and Turbulence*, 10–15 January, 1999, Dallas, TX.

Acevedo, O. and Fitzjarrald, D. R.: 2001, 'The Early Evening Surface-Layer Transition: Temporal and Spatial Variability', *J. Atmos. Sci.* **58**, 2650–2667.

Andren, A.: 1995, 'The Structure of Stably Stratified Atmospheric Boundary Layers: A Large Eddy Simulation Study', *Quart. J. Roy. Meteorol. Soc.* **121**, 961–985.

Arya, S. P. S. and Wyngaard, J. C.: 1975, 'Effects of Baroclinicity of Wind Profiles and the Geostrophic Drag Law for the Convective Planetary Boundary Layer', *J. Atmos. Sci.* **32**, 767–778.

Beets, C. and Koren, B.: 1996, *Large Eddy Simulation with Accurate Implicit Subgrid-Scale Diffusion*, Report NM-R9801, Centrum voor Wiskunde en Informatica, The Netherlands, 25 pp.

Brown, A. R.: 1996, 'Large-Eddy Simulation and Parameterization of the Baroclinic Boundary', *Quart. J. Roy. Meteorol. Soc.* **122**, 1779–1798.

Brown, A. R.: 1999, 'Large-Eddy Simulation and Parameterization of the Effects of Shear on Shallow Cumulus Convection', *Boundary-Layer Meteorol.* **91**, 65–80.

Brown, A., Cederwall, R. T., Chlond, A., Duynkerke, P. G., Golaz, J. C., Khairoutdinov, M., Lewellen, D. C., Lock, A. P., McVean, M. K., Moeng, C.-H., Neggers, R. A., Siebesma, A. P., and Stevens, B.: 2002, 'Large-Eddy Simulation of Diurnal Cycle of Shallow Convection over Land', *Quart. J. Roy. Meteorol. Soc.* **128**, 1075–1093.

Brunt, D.: 1934, *Physical and Dynamical Meteorology*, Cambridge University Press, 411 pp.

Cedeval, R. and Street, R. L.: 1999, 'Turbulence Modification in the Envolving Stable Boundary Layer: A Large-Eddy Simulation', in *13th Symposium on Boundary Layers and Turbulence*, Dallas, TX, American Meteorological Society.

Chlond, A. and Wolkau, A.: 2000: 'Large-Eddy Simulation of a Nocturnal Stratocumulus-Topped Marine Atmospheric Boundary Layer: An Uncertainty Analysis', *Boundary-Layer Meteorol.* **95**, 31–55.

Cuijpers J. W. M. and Duynkerke, P. G.: 1993, 'Large-Eddy Simulation of Trade Wind Cumulus Clouds', *J. Atmos. Sci.* **50**, 3894–3908.

Cushman-Roisin, B.: 1994, *Introduction to Geophysical Fluid Dynamics*, Prentice Hall, 320 pp.

Deardorff, J. W.: 1970: 'Preliminary Results from Numerical Integration of the Unstable Planetary Boundary Layers', *J. Atmos. Sci.* **27**, 1209–1211.

Deardorff, J. W.: 1972, 'Numerical Integration of Neutral and Unstable Planetary Boundary Layers', *J. Atmos. Sci.* **29**, 91–115.

Deardorff, J. W.: 1973a, 'Three-Dimensional Numerical Modeling of the Planetary Boundary Layers', in D. A. Haugen (ed.), *Workshop on Micrometeorology*, American Meteorological Society, pp. 271–311.

Deardorff, J. W.: 1973b, 'The Use of Subgrid Transport Equations in a Three-Dimensional Model of Atmospheric Turbulence', *J. Fluids Eng.* **95**, 429–438.

Deardorff, J. W.: 1974, 'Three-Dimensional Numerical Study of the Height and Mean Structure of a Heated Planetary Boundary Layer', *Boundary-Layer Meteorol.* **7**, 81–106.

Deardorff, J. W.: 1976, 'On the Entrainment Rate of a Stratocumulus-Topped Mixed Layer', *Quart. J. Roy. Meteorol. Soc.* **102**, 563–582.

Deardorff, J. W., Willis, G. E., and Stockton, B. H.: 1980, 'Laboratory Studies of the Entrainment Zone of a Convectively Mixed Layer', *J. Fluid Mech.* **100**, 41–64.

Driedronks, A. G. M.: 1982, 'Models and Observations of the Growth of the Atmospheric Boundary Layer', *Boundary-Layer Meteorol.* **23**, 283–306.

Holton, J. R.: 1972, *An Introduction to Dynamic Meteorology*, Academic Press, 319 pp.

Kim, S.-W., Park, S.-U., and Moeng, C.-H.: 2003, 'Entrainment Processes in the Convective Boundary Layer with Varying Wind Shear', *Boundary-Layer Meteorol.* **108**, 221–245.

Kosovic, B and Curry, J.: 1999, 'Large-Eddy Simulation of a Quasi-Steady Stably-Stratified Atmospheric Boundary Layer', in *13th Symposium on Boundary Layers and Turbulence*, Dallas, TX, American Meteorological Society.

LeMone, M. A., Grossman, R. L., Coulter, R. L., Wesley, M. L., Klazura, G. E., Poulos, G. S., Blumen, W., Lundquist, J. K., Cuenca, R. H., Kelly, S. F., Brandes, E. A., Oncley, S. P., McMillen, R. T., and Hicks, B. B.: 2000, 'Land-Atmosphere Interaction Research, Early Results, and Opportunities in the Walnut River Watershed in Southeast Kansas: CASES and ABLE', *Bull. Amer. Meteorol. Soc.* **81**, 757–779.

Lilly, D. K.: 1968, 'Models of Cloud-Capped Mixed Layers under a Strong Inversion', *Quart. J. Roy. Meteorol. Soc.* **94**, 292–309.

Mahrt, L. J. and Schwerdtfeger, W.: 1970, 'Ekman Spirals for Exponential Thermal Wind', *Boundary-Layer Meteorol.* **1**, 137–145.

Mason, P. J.: 1989, 'Large-Eddy Simulation of the Convective Atmospheric Boundary Layer', *J. Atmos. Sci.* **46**, 1492–1516.

Mason, P. J. and Derbyshire, S. H.: 1990, 'Large-Eddy Simulation of the Stably-Stratified Atmospheric Boundary Layer', *Boundary-Layer Meteorol.* **53**, 117–162.

Moeng, C.-H.: 1984, 'A Large-Eddy Simulation Model for the Study of Planetary Boundary-Layer Turbulence', Part I, *J. Atmos. Sci.* **41**, 2052–3169.

Moeng, C. H.: 1986, 'Large-Eddy Simulation of a Stratus-Topped Boundary-Layer', *J. Atmos. Sci.* **43**, 2862–2900.

Moeng, C. H. and Sullivan, P. P.: 1994, 'A Comparison of Shear and Buoyancy Driven Planetary Boundary Layer Flows', *J. Atmos. Sci.* **51**, 999–1022.

Nieuwstadt, F. T. M.: 1984, 'The Turbulent Structure of the Stable, Nocturnal Boundary Layer', *J. Atmos. Sci.* **41**, 2202–2216.

Nieuwstadt, F. T. M. and Brost, R. A.: 1986, 'The Decay of Convective Turbulence', *J. Atmos. Sci.* **43**, 532–546.

Saiki, E. M., Moeng, C. H., and Sullivan, P. P.: 1999, Large-Eddy Simulation of the Stably Stratified Planetary Boundary Layer', in *13th Symposium on Boundary Layers and Turbulence*, Dallas, TX, American Meteorological Society.

Salby, M. L.: 1996, *Fundamentals of Atmospheric Physics*, Academic Press, 624 pp.

Schemm, C. E. and Lipps, F. B.: 1976, 'Some Results from a Simplified Three-Dimensional Numerical Model of Atmospheric Turbulence', *J. Atmos. Sci.* **33**, 1021–1041.

Schmidt, H. and Schumann, U.: 1989, 'Coherent Structure of the Convective Boundary Layer Derived from Large-Eddy Simulation', *J. Fluid Mech.* **200**, 511–562.

Schumann, U.: 1991, 'Subgrid Length-Scales for Large-Eddy Simulation of Stratified Turbulence', *Theor. Comp. Fluid Dyn.* **2**, 229–290.

Sommeria, G.: 1976, 'Three-Dimensional Simulation of Turbulent Processes in an Undisturbed Trade Wind Boundary Layer', *J. Atmos. Sci.* **33**, 216–241.

Sorbjan, Z.: 1989, *Structure of the Atmospheric Boundary Layer*, Prentice Hall, 399 pp.

Sorbjan, Z.: 1991, 'Evaluation of Local Similarity Functions in the Convective Boundary Layer', *J. Appl. Meteorol.* **30**, 1565–1583.

Sorbjan, Z.: 1995, 'Toward Evaluation of Heat Fluxes in the Convective Boundary Layer', *J. Appl. Meteorol.* **34**, 1092–1098

Sorbjan, Z.: 1996a, 'Reply', 35, *J. Appl. Meteorol.* **34**, 1374–1377.

Sorbjan, Z.: 1996b, 'Numerical Study of Penetrative and "Solid-Lid" Non-Penetrative Convective Boundary Layers', *J. Atmos. Sci.* **53**, 101–112.

Sorbjan, Z.: 1996c, 'Effects Caused by Varying Strength of the Capping Inversion Based on a Large-Eddy Simulation of the Shear-Free Convective Boundary Layer', *J. Atmos. Sci.* **53**, 2015–2024.

Sorbjan, Z.: 1997, 'Decay of Convective Turbulence Revisited', *Boundary-Layer Meteorol.* **82**, 501–515.

Sorbjan, Z.: 1999, 'Similarity of Scalar Fields in the Convective Boundary Layer', *J. Atmos. Sci.* **56**, 2212–2221.

Sorbjan Z.: 2001, 'An Evaluation of Local Similarity on the Top of the Mixed Layer Based on Large-Eddy Simulations', *Boundary-Layer Meteorol.* **101**, 183–207.

Stevens, B., Ackerman, A. S., Albrecht, B. A., Brown, A. R., Chlond, A., Cuxart, J., Duynkerke, P. G., Lewellen, D. C., MacVean, M. K., Neggers, R. A., Sanchez, E., Siebesma, A. P., and Stevens, D. E.: 2001, 'Simulation of Trade Wind Cumuli under a Strong Inversion', *J. Atmos. Sci.* **58**, 1870–1891.

Stevens, B., Moeng, C. H., and Sullivan, P. P.: 1999, 'Large-Eddy Simulations of Radiatively Driven Convection: Sensitivities to the Representation of Small Scales', *J. Atmos. Sci.* **56**, 3963-3984.

Sullivan, P. P., Moeng, C.-H., B, Stevens, B., Lenschow, D.H., and Mayor, S. D.: 1998, 'Structure of the Entrainment Zone Capping the Convective Boundary Layer', *J. Atmos. Sci.* **55**, 3042–3064.

Tennekes, H.: 1973, 'A Model for the Dynamics of the Inversion above a Convective Boundary Layer', *J. Atmos. Sci.* **30**, 558–567.

Tennekes, H.: 1980, 'Basic Entrainment Equations for the Atmospheric Boundary Layer', in *Second International Symposium on Stratified Flows*, The Norwegian Institute of Technology.

Venkatesh, S. and Csanady, G. T.: 1974), 'A Baroclinic Planetary Boundary Layer, and its Application to the Wangara Data', *Boundary-Layer Meteorol.* **5**, 459–473.

Wippermann, F.: 1972, 'Empirical Formulae for the Universal Functions M and N in the Resistance Law for a Barotropic Planetary Bboundary Layer and Diabatic Planetary Boundary Layer', *Beitr. Phys. Atmosph.* **45**, 305–311.

Wippermann, F. and Yordanov, D.: 1972, 'A Note on the Rossby Similarity for Flows of Barotropic Planetary Boundary Layers', *Beitr. Phys. Atmosph.* **45**, 66–71.

Wyngaard, J. C., Arya, S. P. S., and Cote, O. R.: 1974, 'Some Aspects of the Structure of Convective Planetary Boundary Layers', *J. Atmos. Sci.* **31**, 747–754.

Yordanov, D. and Wipperman, F.: 1972', 'The Parameterization of Turbulent Fluxes of Momentum, Heat and Moisture at the Ground in a Baroclinic Planetry Boundary Layer', *Beitr. Phys. Atmosph.* **45**, 58–65.

Zilitinkevich, S. S.: 1991, *Turbulent Penetrative Convection*, Avebury Technical, Aldershot, 179 pp.